



## Renoprotective effects of brown adipose tissue activation in diabetic mice

Cai, Ying-Ying; Zhang, Hong-Bin; Fan, Cun-Xia; Zeng, Yan-Mei; Zou, Shao-Zhou; Wu, Chun-Yan; Wang, Ling; Fang, Shu; Li, Ping; Xue, Yao-Ming; Guan, Mei-Ping

*Published in:*  
Journal of Diabetes

*DOI:*  
[10.1111/1753-0407.12938](https://doi.org/10.1111/1753-0407.12938)


*Publication date:*  
2019

*Document version*  
Publisher's PDF, also known as Version of record

*Document license:*  
[CC BY-NC-ND](https://creativecommons.org/licenses/by-nc-nd/4.0/)

*Citation for published version (APA):*  
Cai, Y-Y., Zhang, H-B., Fan, C-X., Zeng, Y-M., Zou, S-Z., Wu, C-Y., ... Guan, M-P. (2019). Renoprotective effects of brown adipose tissue activation in diabetic mice. *Journal of Diabetes*, 11(12), 958-970. <https://doi.org/10.1111/1753-0407.12938>

# Renoprotective effects of brown adipose tissue activation in diabetic mice

Ying-Ying Cai<sup>1,2\*</sup> | Hong-Bin Zhang<sup>3\*</sup> | Cun-Xia Fan<sup>1,4</sup> | Yan-Mei Zeng<sup>1</sup> |  
Shao-Zhou Zou<sup>1</sup> | Chun-Yan Wu<sup>1</sup> | Ling Wang<sup>1</sup> | Shu Fang<sup>1</sup> | Ping Li<sup>1</sup> |  
Yao-Ming Xue<sup>1</sup> | Mei-Ping Guan<sup>1</sup> 

<sup>1</sup>Department of Endocrinology and Metabolism, Nanfang Hospital, Southern Medical University, Guangzhou, China

<sup>2</sup>Department of Birth Control, Women and Children's Hospital, School of Medicine, Xiamen University, Xiamen, China

<sup>3</sup>Department of Biomedical Sciences, University of Copenhagen, Copenhagen, Denmark

<sup>4</sup>Department of Endocrinology and Metabolism, Hainan General Hospital, Haikou, China

## Correspondence

Mei-Ping Guan, Department of Endocrinology and Metabolism, Nanfang Hospital, Southern Medical University, 1838 Guangzhou Avenue North, Guangzhou, Guangdong 510515, China.  
Email: mpguan@163.com

## Funding information

National Natural Science Foundation of China, Grant/Award Numbers: 81870612, 81628004, 31400992, 81470047; Science and Technology Planning Project of Guangdong Province, Grant/Award Number: 2013B022000061; Wu Jieping Medical Foundation, Grant/Award Number: 320.6750.15198

## Highlights

- This study demonstrates that of brown adipose tissue (BAT) with CL316,243 attenuates the progress of diabetic kidney disease (DKD).
- Mechanistically, the activation of BAT improved concentrations of circulating adipokines and microRNAs, which further affected the diabetic kidney and reactivated the AMP-activated protein kinase/sirtuin 1/peroxisome proliferator-activated receptor- $\gamma$  coactivator-1 $\alpha$  signaling pathway.
- The data suggest that BAT activation could be a novel therapeutic approach in the treatment of DKD.

## Abstract

**Background:** Brown adipose tissue (BAT) has been regarded as a potential target organ to combat obesity and related metabolic disorders. However, the effect of BAT activation on the development of diabetic kidney disease (DKD) remains unclear.

**Methods:** Diabetic mice were induced by streptozotocin (STZ) combined with a high-fat diet. To activate BAT, mice were administered 1 mg/kg per day, i.p., CL316,243, a  $\beta_3$ -adrenergic receptor agonist, for 4 weeks. Blood glucose, serum lipids, adipokines, 24-hour urinary albumin, 8-hydroxydeoxyguanosine (8-OHdG), and circulating microRNA (miRNA) levels were analyzed, in addition to renal pathology. Histological changes (fibrosis, inflammation) were evaluated in the kidneys, as was the expression of oxidative stress-related genes. Renal signaling pathways (fibroblast growth factor [Fgf]21/ $\beta$ -klotho/FGF receptor 1c and AMP-activated protein kinase[AMPK]/sirtuin 1 [Sirt1]/peroxisome proliferator-activated receptor- $\gamma$  coactivator-1 $\alpha$  [Pgc1 $\alpha$ ]) were also evaluated.

**Results:** Compared with untreated STZ-diabetic mice, CL316,243 treatment reduced blood glucose, albeit not significantly ( $20.58 \pm 3.55$  vs  $23.60 \pm 3.90$  mM), and significantly decreased triglycerides and low-density lipoprotein cholesterol and increased high-density lipoprotein cholesterol. Simultaneously,

\*These authors contributed equally to this work.

This is an open access article under the terms of the Creative Commons Attribution-NonCommercial-NoDerivs License, which permits use and distribution in any medium, provided the original work is properly cited, the use is non-commercial and no modifications or adaptations are made.

© 2019 The Authors. *Journal of Diabetes* published by John Wiley & Sons Australia, Ltd and Ruijin Hospital, Shanghai Jiaotong University School of Medicine.



BAT activation significantly decreased 24-hour urinary albumin ( $34.21 \pm 6.28$  vs  $70.46 \pm 15.81$   $\mu\text{g}/24$  h;  $P < 0.05$ ) and 8-OHdG, improved renal fibrosis, inflammation, and oxidative stress, and ameliorated renal morphological abnormalities. In addition to enhancing BAT activity, CL316,243 significantly increased serum adiponectin concentrations and renal Fgf21 sensitivity, and reactivated the renal AMPK/Sirt1/Pgc1 $\alpha$  signaling pathway. Furthermore, CL316,243 treatment increased levels of some circulating miRNAs and downregulated expression of their target genes in the kidney.

**Conclusions:** Activating BAT could improve kidney injury in diabetic mice via metabolic improvements and renal AMPK activation by beneficial adipokines and miRNAs.

#### KEY WORDS

adipokine, brown adipose tissue, CL316,243, diabetic kidney disease, microRNA

## 1 | INTRODUCTION

Diabetic kidney disease (DKD) is one of the major causes of end-stage renal disease (ESRD). Current treatments, including various pharmacological strategies and changes in lifestyle, are only partially effective in preventing progression of DKD.<sup>1</sup> It is very important to explore new targets to improve the outcomes.

Lipotoxicity has been implicated in the pathophysiology of DKD.<sup>2</sup> Recent studies have shown that various adipokines, such as adiponectin and fibroblast growth factor (FGF) 21, are involved in the regulation of renal metabolism.<sup>3</sup> In addition, adipose-derived circulating microRNAs (miRNAs) have been demonstrated to regulate the metabolism of other tissues.<sup>4</sup> Various miRNAs play an important role in the kidney.<sup>5</sup> These findings reveal that adipose tissue may be closely related to the development of DKD. Unlike white adipose tissue, brown adipose tissue (BAT) is a mitochondria-rich tissue that is specialized in non-shivering thermogenesis through consumption of fatty acids and glucose.<sup>6</sup> Many previous rodent studies have revealed that activation of BAT for 4 weeks can regulate energy metabolism and glucose homeostasis.<sup>7,8</sup> In 2009, BAT was found to be functional in adult humans,<sup>9</sup> and was recently proved to be activated in humans by  $\beta_3$ -adrenergic receptor agonists.<sup>10</sup> Activation of BAT has been considered to be associated with immunity against obesity, diabetes, and related metabolic diseases.<sup>11</sup> In addition, as an endocrine organ, BAT can secrete adipokines to regulate metabolism.<sup>12</sup> Chronic stimulation of BAT for 30 days also contributes to the release of adipokines, which have beneficial effects on the kidneys.<sup>13,14</sup> Together, these findings suggest that activation of BAT may have beneficial effects in preventing the

development of DKD. However, the relationship between BAT and DKD has not been reported before.

In the present study we administered the  $\beta_3$ -adrenergic receptor agonist CL316,243 to stimulate BAT in type 2 diabetic (T2D) mice to investigate the effects of BAT activation on kidney disease. Our hypothesis was that BAT activation would attenuate the development of DKD by improving metabolism and increasing levels of beneficial adipokines and miRNAs, which could activate downstream signaling pathways in the kidney.

## 2 | METHODS

### 2.1 | Animals

Male C57BL/6J mice, aged 6 weeks ( $n = 30$ ), were purchased from Guangdong Medical Laboratory Animal Center (Guangzhou, China). All animals were maintained in a specific pathogen-free (SPF) barrier facility at Southern Medical University (Guangzhou, China). Mice were kept at 22°C under a 12-hour light-dark cycle and had free access to water and diet. All animal experiments were conducted in accordance with the regulation of the Animal Care and Use Committee of the Southern Medical University.

### 2.2 | Induction of the diabetic mouse model and CL316,243 treatment

Mice were randomly divided into two groups and fed either a chow diet (Control) or high-fat diet (HFD; 5.24 kcal/g; 60% kcal from fat, 20% kcal from carbohydrate; Guangdong Medical Laboratory Animal Center). To induce hyperglycemia, after 4 weeks of feeding the HFD, mice ( $n = 22$ ) received a single intraperitoneal injection of streptozotocin

(STZ; 120 µg/g body weight in 10 mM sodium citrate buffer, pH 4.5; S0130; Sigma, Shanghai, China),<sup>15</sup> whereas the mice in the Control group (n = 8) were injected with an equivalent volume of citrate buffer. Mice were considered diabetic when their blood glucose concentrations exceeded 250 mg/dL. At Week 8, diabetic mice (n = 18) were randomly divided into two groups, a diabetic control group (DM-Con; n = 9) and a diabetic group treated with the β<sub>3</sub>-adrenergic receptor agonist CL316,243 (DM + CL; n = 9). Mice in the DM + CL group were administered 1 mg/kg, i. p., CL316,243 daily for 4 weeks, whereas mice in the DM-Con group received saline only. Throughout the experiment, the Control and diabetic mice were fed chow diet and the HFD, respectively. Food intake, body weight, and blood glucose were measured every week. At Week 12, blood was collected from the left ventricle under anesthesia (sodium pentobarbital of 50 mg/kg through intraperitoneal injection) after 4 hours of fasting; serum was stored at -80°C until analysis. Mice were killed by cervical dislocation, and adipose tissues and kidneys were harvested and immediately frozen in liquid nitrogen until further analysis.

### 2.3 | Assessment of renal function, oxidative stress, and Fgf21 concentrations

At Weeks 8, 10, and 12, mice were placed individually in metabolic cages to collect 24-hour urine samples. Urinary albumin and 8-hydroxydeoxyguanosine (8-OHdG) concentrations were measured by ELISA (Bethyl Laboratories, Montgomery, Texas; Cusabio, Barksdale, USA, respectively). Serum creatinine (Cr) was measured using a commercially available kit (Nanjing Jiancheng Bioengineering Institute, Nanjing, China), and FGF21 protein in the renal cortex was determined by ELISA (Elabscience Biotechnology, Wuhan, China).

### 2.4 | Measurement of serum parameters

During the experiment, random blood glucose levels were measured using an Accu-Chek glucose monitor (Roche, Shanghai, China). Serum adiponectin and Fgf21 concentrations were determined by ELISA (Elabscience Biotechnology). Triglycerides (TG), high-density lipoprotein cholesterol (HDL-C) and low-density lipoprotein cholesterol (LDL-C) were measured using commercially available kits (Nanjing Jiancheng Bioengineering Institute).

### 2.5 | Extraction of ribonucleic acid (RNA) and quantitative real-time polymerase chain reaction (qRT-PCR)

The renal cortex and adipose tissues were snap frozen in liquid nitrogen, and RNA was extracted with TRIzol (Takara,

Dalian, China). The quality of the RNA was determined using a NanoDrop ND-1000 Spectrophotometer (Thermo Fisher Scientific, Waltham, Massachusetts). The cDNA was synthesized by using an M-MLV Kit (Invitrogen, Carlsbad, California). Real-time quantitative polymerase chain reaction (qPCR) was performed in a Roche Lightcycler 480II (Roche, Basle, Switzerland) using a SYBR Green qPCR Kit (Takara). Relative gene expression was calculated using the 2<sup>-ΔΔCt</sup> method and 18 s as an internal control.<sup>16</sup> The primers used are listed in Table 1.

### 2.6 | Isolation of miRNAs and real-time qPCR

Serum total RNA was isolated using the miRcute serum/plasma miRNA isolation kit (TianGen, Beijing, China) and reverse transcribed using a miRNA First-Strand cDNA Synthesis kit (TianGen) according to the manufacturer's instructions. Because of the lack of a stable endogenous serum miRNA, samples were spiked with a synthetic *Caenorhabditis elegans* mir-39 miRNA mimic (cel-mir-39) as a control to monitor changes in RNA recovery. The real-time qPCR was performed in a Roche LightCycler480II using the miRcute miRNA Detection Kit (TianGen). Relative expression of target miRNAs was calculated using the comparative 2<sup>-ΔΔCt</sup> method with external control. In virtue of the lack of a stable endogenous serum miRNA, samples were spiked with a synthetic *C. elegans* mir-39 miRNA mimic (cel-mir-39) as a control to monitor changes in RNA recovery. cel-mir-39 was the external control. Primers for miR-26a, miR-30b, miR-30c, miR99a, miR100, miR181a, and the external control were designed by the authors. Primer sequences of these miRs as follows: miR-30b-5p: 5'-GC GTCCTGTAACATCCTACACTCAGCT-3' miR-99a-5p: 5'-GCGTAACCCGTAGATCCGATCTTGTG-3' miR-100-5p: 5'-GCGTAACCCGTAGATCCGAACCTTGTG-3' miR-181a-5p: 5'-GCGTCCAACATTCAACGCTGTCGGTGAGT-3' The universal reverse primer and primers for miR-26a and miR-30c were purchased from TianGen (Beijing, China).

### 2.7 | Western blotting

Total protein from the renal cortex and adipose tissues was extracted using RIPA Lysis Buffer (Beyotime, Shanghai, China), and protein concentrations were measured by the bicinchoninic acid assay (Takara). Proteins (40 µg) were electrophoresed by 10%-15% sodium dodecyl sulfate-polyacrylamide gel electrophoresis (Bio-Rad, Hercules, California) and then transferred to polyvinylidene difluoride membranes (Merck Millipore, Billerica, Massachusetts). After membranes had been blocked, with 5% non-fat milk or 5% BSA they were hybridized overnight at 4°C with primary antibodies against transforming growth factor (Tgf)-β1 (1: 500 dilution; Santa Cruz Biotechnology, Santa Cruz,

**TABLE 1** Primer sequences used for real-time quantitative polymerase chain reaction

Gene name	Gene symbol	Primers (5'-3')
Fibronectin	<i>Fn</i>	Forward: TAGCCCTGTCCAGGAGTTCA Reverse: CTGCAAGCCTTCAATAGTCA
Collagen 1	<i>Col1</i>	Forward: GCAGGAGGTTTCGGCTAAGT Reverse: GCAACAAAGTCCGCGTATCC
Transforming growth factor- $\beta$ 1	<i>Tgfb1</i>	Forward: CCACCTGCAAGACCATCGAC Reverse: CTGGCGAGCCTTAGTTTGAC
Tumor necrosis factor- $\alpha$	<i>Tnfa</i>	Forward: CATCTTCTCAAAATTCGAGTGACAA Reverse: TGGGAGTAGACAAGGTACAACCC
Interleukin-1 $\beta$	<i>Il-1<math>\beta</math></i>	Forward: GTCTTTCCCGTGACCTTC Reverse: ATCTCGGAGCCTGTTAGTGC
Uncoupling protein 1	<i>Ucp1</i>	Forward: AGGCTTCCAGTACCATTAGGT Reverse: CTGAGTGAGGCAAAGCTGATTT
Peroxisome proliferator-activated receptor- $\gamma$ coactivator-1 $\alpha$	<i>Pgc1<math>\alpha</math></i>	Forward: CCCTGCCATTGTTAAGACC Reverse: TGCTGCTGTTCTGTTTTTC
Cd36	<i>Cd36</i>	Forward: TGTGTTTGGAGGCATTCTCA Reverse: TTTTGCACGTCAAAGATCCA
Adipose triglyceride lipase	<i>Atgl</i>	Forward: TGTGGCCTCATTCTCTCTAC Reverse: TCGTGGATGTTGGTGGAGCT
Cytochrome c oxidase subunit 2	<i>Cox2</i>	Forward: CCATCCCAGGCCGACTAA Reverse: AATTTTCAGAGCATTGGCCATAGA
Klotho beta	<i>Klb</i>	Forward: CAGGCCCATTTGTTACCTTGT Reverse: CTCCAAAGGTCTGGAAGCAG
Fibroblast growth factor receptor 1c	<i>Fgfr1c</i>	Forward: AATACCACCGACAAGGAAATGG Reverse: AGTTACCCGCCAAGCACGTA
	<i>18S</i>	Forward: AGCCTGCGGCTTAATTTGAC Reverse: CAACTAAGAACGGCCATGCA

California), collagen 1 (Col1; 1:200 dilution; Abcam, Cambridge, MA), fibronectin (Fn; 1: 500 dilution; R&D, Minneapolis, MN), tumor necrosis factor (Tnf)- $\alpha$  (1: 500 dilution; ABclonal, Boston, MA), NADPH oxidase 1 (Nox1; 1: 500 dilution; GeneTex, Irvine, CA), superoxide dismutase 1 (Sod1; 1: 200 dilution; Santa Cruz Biotechnology), NAD(P)H dehydrogenase 1 (Nqo1; 1: 200 dilution; Santa Cruz Biotechnology), phosphorylated (p-) AMP-activated protein kinase (AMPK; 1: 1000 dilution; CST, Danvers, MA), total AMPK (1: 500 dilution; CST), sirtuin 1 (Sirt1; 1: 2000 dilution; Abcam), peroxisome proliferator-activated receptor- $\gamma$  coactivator-1 $\alpha$  (Pgc1 $\alpha$ ; 1: 1000 dilution; Novus Biologicals, Littleton, CO), uncoupling protein 1 (Ucp1) (1: 500 dilution; Santa Cruz Biotechnology), and  $\beta$ -actin (1: 500; ZSGB-BIO, Beijing, China). The membranes were then incubated with an appropriate horseradish peroxidase-conjugated secondary antibody for 1 hour, whose signal was visualized using enhanced chemiluminescence (ECL)

reagents (Tanon, Shanghai, China) and quantified by GelPro32 (Media Cybernetics, Silver Springs, MD, USA). The membranes were washed for 3 times (8 minutes per time) with Tris-buffered saline containing 0.1% Tween-20 (TBST) after the overnight incubation with the primary antibodies. Then the membranes were incubated with secondary antibody.

## 2.8 | Histological examination

Renal tissues were fixed for 48 hours with 4% paraformaldehyde, dehydrated, embedded in paraffin, and cut into 4- $\mu$ m slices, before being stained with periodic acid-Schiff (PAS) and Masson's trichrome to assess mesangial matrix expansion and collagen deposition, respectively. More than 25 glomeruli per group were counted, and the mean was used for analysis. All sections were evaluated

under an Olympus (Tokyo, Japan) BX40 upright light microscope.

## 2.9 | Statistical analysis

Data are expressed as the mean  $\pm$  SEM. Two-tailed Student's *t* tests were used to compare two independent groups, and one-way analysis of variance (ANOVA) was used to examine the significance of differences among three independent groups. Dunnett's test or the least significant difference (LSD) test was used for multiple comparisons. Statistical analyses were performed in SPSS 20.0 (IBM Corp., Armonk, New York).  $P < 0.05$  was considered significant.

## 3 | RESULTS

### 3.1 | Effects of CL316,243 on metabolic parameters in diabetic mice

Blood glucose concentrations were higher in diabetic than Control mice (by approximately 3-fold). There was a non-significant decrease in blood glucose concentrations in mice in the DM + CL compared with DM-Con group ( $20.58 \pm 3.55$  vs  $23.6 \pm 3.9$  mM, respectively; Figure 1A). As shown in Figure 1B, serum TG ( $1.32 \pm 0.19$  vs  $0.53 \pm 0.02$  mM) and LDL-C ( $1.00 \pm 0.10$  vs  $0.21 \pm 0.04$  mM) concentrations were higher in the DM-Con than Control group ( $P < 0.001$ ), and this was reversed by CL316,243 treatment ( $P < 0.01$ ). In contrast, serum HDL-C was higher in the DM + CL group than in the Control and DM-Con groups ( $4.44 \pm 0.28$  vs  $2.84 \pm 0.17$  and  $3.32 \pm 0.23$  mM, respectively;  $P < 0.01$ ). Kidney weight and the kidney weight/body weight ratio

were higher in the DM-Con group than in the Control and DM + CL groups ( $P < 0.05$ ; Table 2). In addition, food intake was increased in the DM-Con group compared with the Control group ( $P < 0.01$ ). However, there was a obvious increase in food intake in DM + CL group compared with the Control and DM-Con groups ( $P < 0.01$ ; Table 2).

### 3.2 | Effects of CL316,243 on 24-hour urinary albumin and 8-OHdG

Urinary albumin excretion was higher in diabetic than Control mice (by approximately 7fold). By 4 weeks after CL316,243 treatment, there was a decrease in urinary albumin excretion in the DM + CL compared with DM-Con group ( $34.21 \pm 6.28$  vs  $70.46 \pm 15.81$   $\mu\text{g}/24$  h, respectively;  $P < 0.05$ ; Figure 2A). Consistent with the results above, high level of urinary 8-OHdG in diabetic mice was decreased by CL316,243 treatment significantly ( $P < 0.001$ ; Figure 2B).

### 3.3 | Effects of CL316,243 on interscapular BAT and epididymal adipose tissues

There were decreases in both Ucp1 mRNA and protein in the BAT of DM-Con compared with Control mice ( $P < 0.05$ ), and these levels were restored by CL316,243 treatment (Figure 3B,C). In addition, compared with DM-Con group, CL316,243 treatment of diabetic mice increased the expression of the mitochondrial and fatty acid metabolism-related genes *Pgc1 $\alpha$* , *Cd36*, and adipose triglyceride lipase (*Atgl*) in epididymal adipose tissue (Figure 3A).

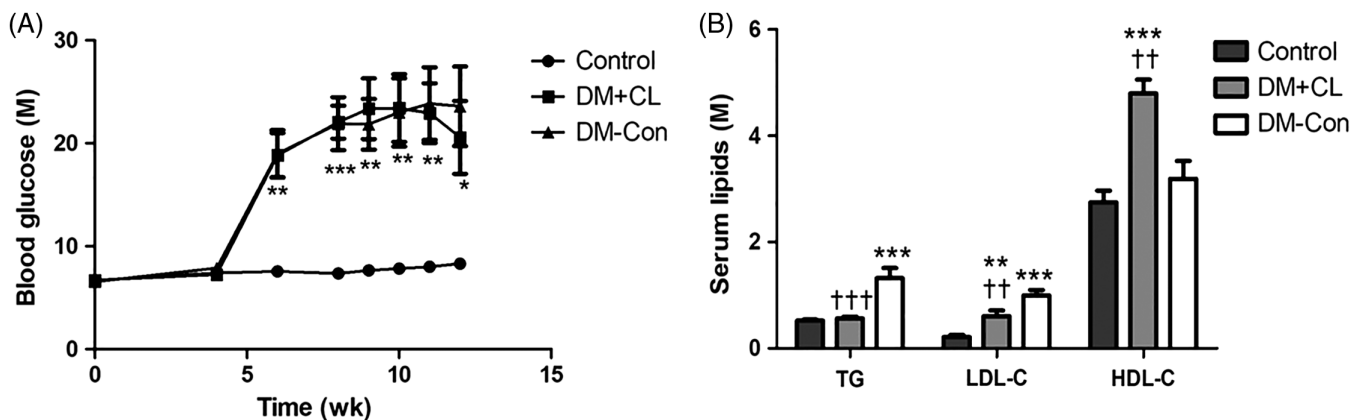


**FIGURE 1** Effects of CL316,243 on A, blood glucose and B, serum lipids in diabetic mice. Data are the mean  $\pm$  SEM ( $n = 7-9$  per group). \* $P < 0.05$ , \*\* $P < 0.01$ , \*\*\* $P < 0.001$  compared with the control group; †† $P < 0.01$ , ††† $P < 0.001$  compared with the diabetic control (DM-Con) group. DM + CL, diabetic mice treated with CL316,243; HDL-C, high-density lipoprotein cholesterol; LDL-C, low-density lipoprotein cholesterol; TG, triglycerides

**TABLE 2** Biochemical and physical parameters of experimental animals at Week 12

Parameters	Control	DM + CL	DM-Con
BW (g)	29.91 ± 0.97	30.51 ± 0.55	29.24 ± 0.70
KW (g)	0.20 ± 0.02	0.22 ± 0.01 <sup>†</sup>	0.27 ± 0.02 <sup>**</sup>
KW/BW (×10 <sup>-3</sup> )	6.40 ± 0.42	6.94 ± 0.37 <sup>††</sup>	9.03 ± 0.49 <sup>**</sup>
RBG (mM) <sup>2</sup>	8.30 ± 0.46	20.58 ± 3.55 <sup>*</sup>	23.6 ± 3.87 <sup>**</sup>
Food intake (kcal/day per mouse)	11.82 ± 0.31	18.92 ± 0.80 <sup>***††</sup>	15.72 ± 0.50 <sup>**</sup>
Serum Cr (μM)	22.79 ± 6.79	23.4 ± 5.43	24.65 ± 5.25
Urine volume (mL)	1.84 ± 0.22	2.77 ± 1.20 <sup>†</sup>	11.50 ± 2.09 <sup>*</sup>

Data are the mean ± SEM (n = 7–9 per group).

BW, body weight; Cr, creatinine; DM + CL, diabetic mice treated with CL316,243; KW, kidney weight; RBG, random blood glucose.

\**P* < 0.05; \*\**P* < 0.01; \*\*\**P* < 0.001 compared with the control (normal) group; <sup>†</sup>*P* < 0.05; <sup>††</sup>*P* < 0.01 compared with the diabetic control (DM-Con) group.

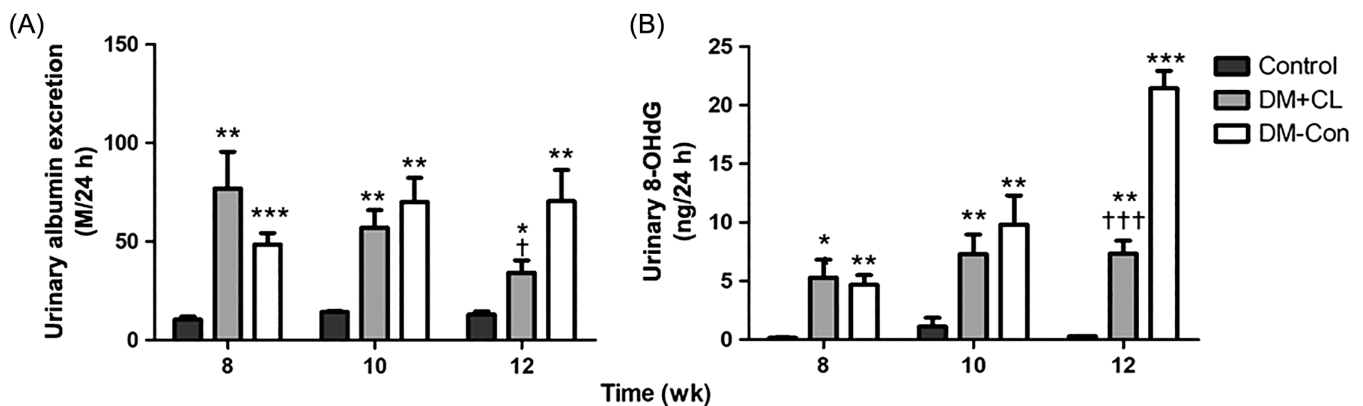


**FIGURE 2** Effects of CL316,243 on 24-h urinary A, albumin excretion and B, 8-hydroxydeoxyguanosine (8-OHdG) concentrations in diabetic mice. Data are the mean ± SEM (n = 7–9 per group). \**P* < 0.05, \*\**P* < 0.01, \*\*\**P* < 0.001 compared with the control group; <sup>†</sup>*P* < 0.05, <sup>††</sup>*P* < 0.01, <sup>†††</sup>*P* < 0.001 compared with the diabetic control (DM-Con) group. DM + CL, diabetic mice treated with CL316,243

### 3.4 | Systemic and renal adipokine expression

Serum adiponectin concentrations were lower in DM-Con than Control mice, but were restored by CL316,243 treatment (*P* < 0.01; Figure 4A). In contrast, serum Fgf21 concentrations were upregulated in DM-Con compared with Control mice (*P* < 0.001), and were not affected by CL316,243 treatment (Figure 4B). In renal cortical tissue, Fgf21 protein expression was in accordance with serum concentrations (Figure 4C). Interestingly, there were significantly increases in Fgf21-related components, including β-klotho and FGF receptor1c (Fgfr1c), in DM-Con compared with Control mice, which were abrogated by CL316,243 treatment (*P* < 0.05; Figure 4D).

### 3.5 | Effects of CL316,243 on serum miRNAs and related target genes in the kidney

Some circulating miRNAs, such as miR-26a, miR-30b, miR-30c, miR-99a, miR-100, and miR-181a, were increased

in diabetic mice. Three of these miRNAs (miR-30b, miR-30c, and miR-99a) were increased in the DM-CL group compared with the other two groups (*P* < 0.05; Figure 5A). Based on the present and previous studies,<sup>16–19</sup> four (Ctgf, Snail1, Nox4, Egr1) candidate related genes in the kidney were identified and tested, namely connective tissue growth factor (Ctgf), snail family zinc finger 1 and early growth response factor 1 (Egr1), the 3'-untranslated region of which could be targeted by miR-26a, miR-30b, miR-30c, miR-99a, and miR-181a. The renal expression of these target genes, verified to be associated with renal fibrosis,<sup>20,21</sup> was suppressed by CL316,243 treatment compared with that in the DM-Con group (*P* < 0.05; Figure 5B).

### 3.6 | Effects of CL316,243 on renal fibrosis, inflammation, and oxidative stress-related molecules

The mRNA expression of fibrotic markers, namely *Tgfb1*, *Coll1*, and *Fn*, and inflammatory markers, namely *Tnfa* and

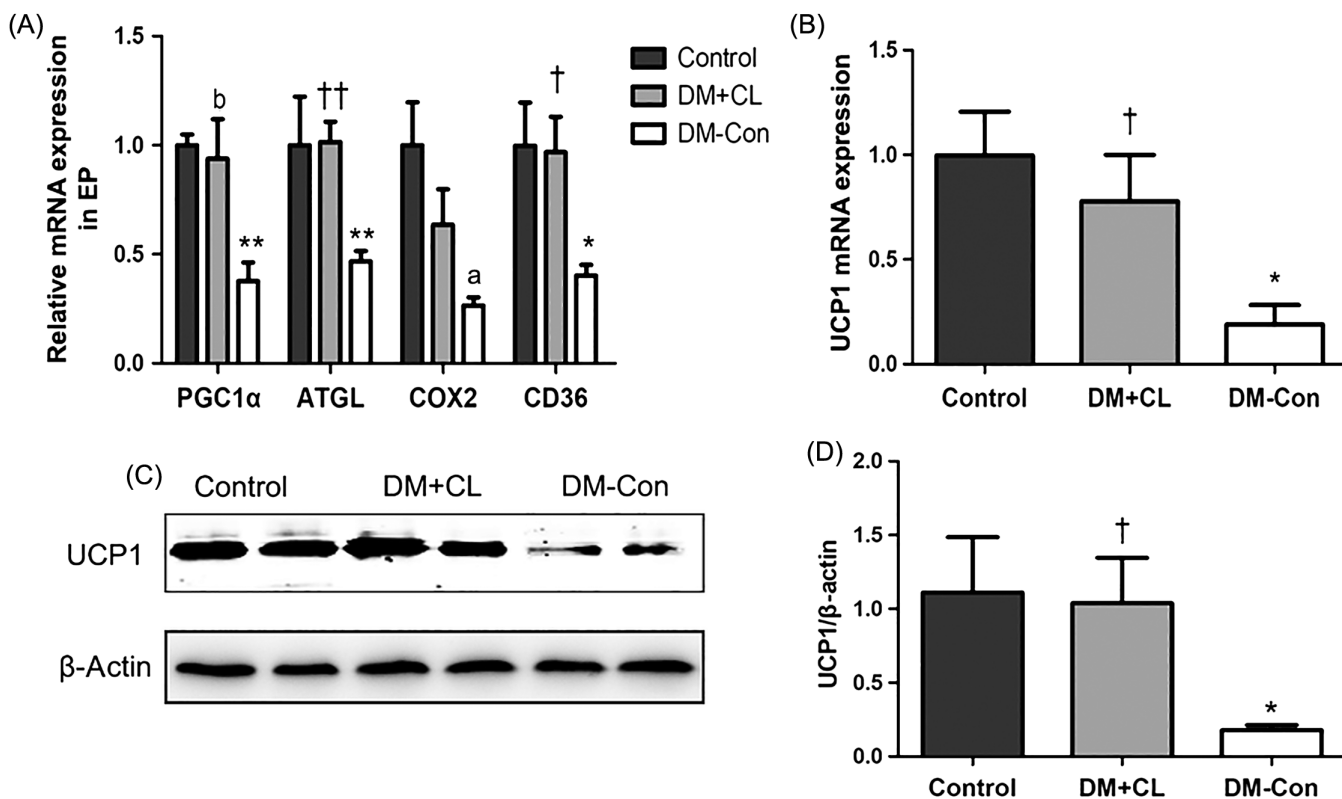


**FIGURE 3** Effects of CL316,243 on relative mRNA expression of A, mitochondrial and thermogenic genes in epididymal adipose tissues (EP) and B, *Ucp1* in interscapular brown adipose tissue (BAT) in diabetic mice. Control, non-diabetic mice; DC-Con, diabetic control mice; DM + CL, diabetic mice treated with CL316,243; *Pgc1 $\alpha$* , peroxisome proliferator-activated receptor- $\gamma$  coactivator-1 $\alpha$ ; *Atgl*, adipose triglyceride lipase; *Cox2*, cytochrome oxidase subunit 2; *Cd36*, cluster of differentiation 36. C Representative western blot for *Ucp1* protein in interscapular BAT and D, densitometric analysis. Data are the mean  $\pm$  SEM (n = 7-9 per group). \* $P$  < 0.05, \*\* $P$  < 0.01 compared with Control; † $P$  < 0.05, †† $P$  < 0.01 compared with the DM-Con group. <sup>a</sup> $P$  = 0.074, <sup>b</sup> $P$  = 0.072 compared with Control

*Il-1 $\beta$* , was increased in DM-Con compared with Control mice ( $P$  < 0.05; Figure 6A). Furthermore, western blotting assays revealed that protein levels were consistent with mRNA expression (Figure 6B–F). However, the increased production of Tg $\beta$ 1, Coll1, Fn, and Tnf $\alpha$  observed in DM-Con mice was significantly attenuated by CL316,243 treatment ( $P$  < 0.05; Figure 6B–F).

Western blotting analysis showed that Sod1 and Nqo1 levels were reduced in DM-Con compared with Control mice, but that CL316,243 treatment enhanced renal Sod1 and Nqo1 expression ( $P$  < 0.05; Figure 6B,H–I). Expression of renal NADPH oxidase 1 (Nox1) was increased in DM-Con compared with Control mice, and was reduced by CL316,243 treatment ( $P$  < 0.05; Figure 6B,G).

### 3.7 | Effects of CL316,243 on renal histological changes

More serious collagen accumulation was observed in DM-Con than Control mice, which was improved by CL316,243 treatment ( $P$  < 0.001; Figure 7B,D). Similarly, there was an increase in fractional mesangial area in DM-Con compared

with Control mice, and the mesangial expansion was obviously improved in the CL316,243-treated group ( $P$  < 0.001; Figure 7A,C).

### 3.8 | Renal expression of p-AMPK (Thr<sup>172</sup>), total AMPK, Sirt1, and Pgc1 $\alpha$

As shown in Figure 8, the ratio of p-AMPK (Thr<sup>172</sup>)/total AMPK and Sirt1 and Pgc1 $\alpha$  levels were markedly decreased in DM-Con compared with Control mice ( $P$  < 0.05). However, the CL316,243 treatment reversed the decreases in the p-AMPK (Thr<sup>172</sup>)/total AMPK ratio and Sirt1 and Pgc1 $\alpha$  levels.

## 4 | DISCUSSION

In the present study we verified the beneficial renal effects of BAT activation in diabetic mice, which were mediated by improvements in systemic and renal metabolism. Chronic stimulation of BAT did not improve glycemic control in diabetic mice, as reported previously.<sup>8</sup> This apparent



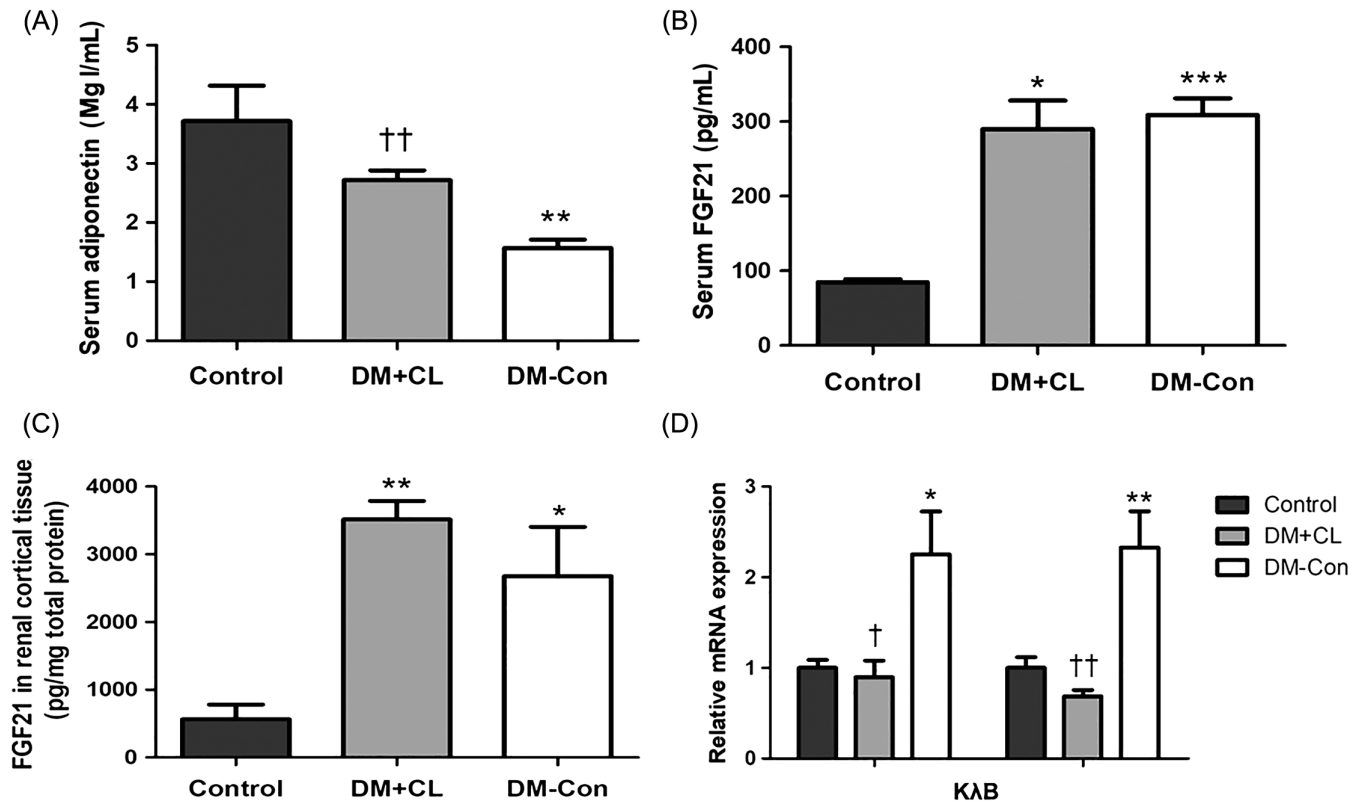


**FIGURE 4** Effects of CL316,243 on serum adipokines (adiponectin and fibroblast growth factor [FGF] 21) and renal expression of Fgf21 components in diabetic mice. A, Serum adiponectin and B, serum Fgf21 concentrations; C, Fgf21 protein and D, relative expression of  $\beta$ -klotho (*Klb*) and FGF receptor 1c (*Fgfr1c*) mRNA in renal cortical tissues. Data are the mean  $\pm$  SEM (n = 6 per group). \* $P$  < 0.05, \*\* $P$  < 0.01, \*\*\* $P$  < 0.001 compared with control (non-diabetic) mice; † $P$  < 0.05, †† $P$  < 0.01 compared with the diabetic control (DM-Con) group. DM + CL, HFD combined with STZ-induced diabetic mice treated with CL316,243

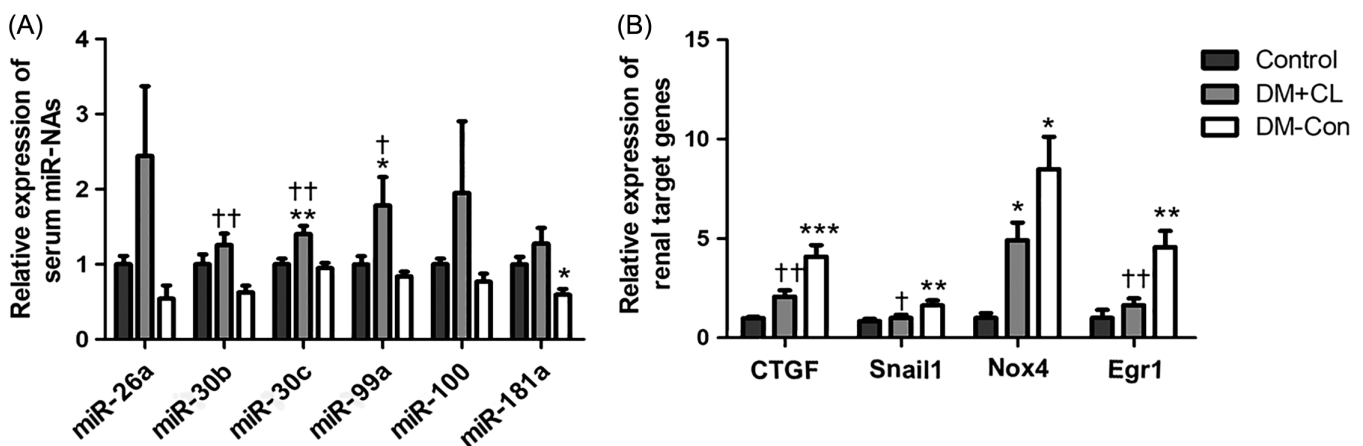


**FIGURE 5** Effects of CL316,243 on serum microRNAs (miR) and renal expression of target genes in diabetic mice. A, Relative expression of miR-26a, miR-30b, miR-30c, miR-99a, miR-100 and miR-181a extracted from the serum of non-diabetic (Control), streptozotocin-induced diabetic (DM-Con), and CL316,243-treated diabetic (DM + CL) mice. B, Relative mRNA expression of connective tissue growth factor (*Ctgf*), *Snail1*, *Nox4*, and early growth response factor 1 (*Egr1*) in renal cortical tissues. Data are the mean  $\pm$  SEM (n = 6 per group). \* $P$  < 0.05, \*\* $P$  < 0.01, \*\*\* $P$  < 0.001 compared with Control; † $P$  < 0.05, †† $P$  < 0.01 compared with the DM-Con group

discrepancy may be due to differences in animal models and interventions. In addition, in contrast to expectations, the body weight of DM-Con mice was not higher than that of

Control mice in the present study, whereas the body weight of CL316,243-treated mice exhibited a tendency to be greater than that of DM-Con mice at the end of the study.

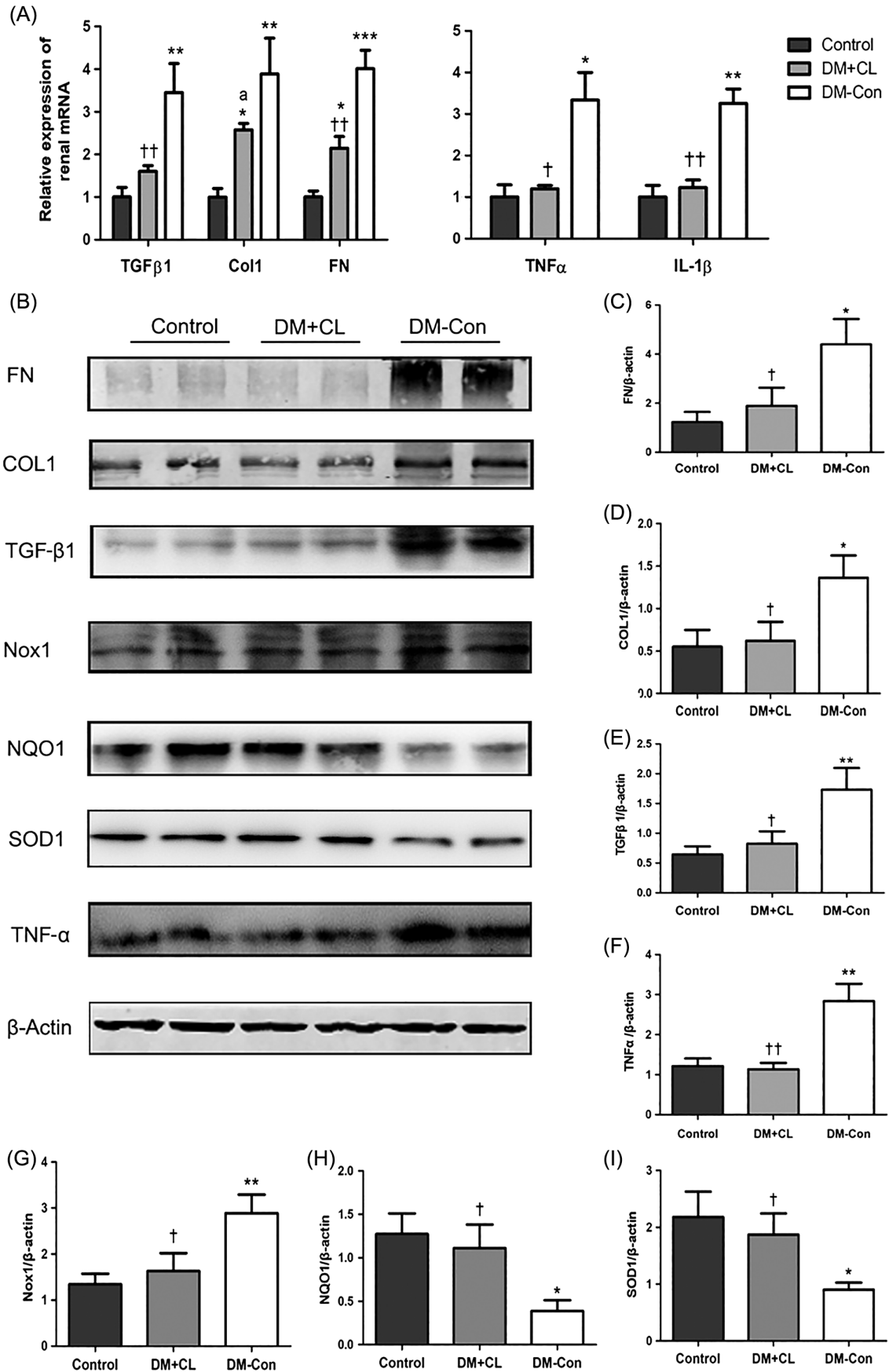
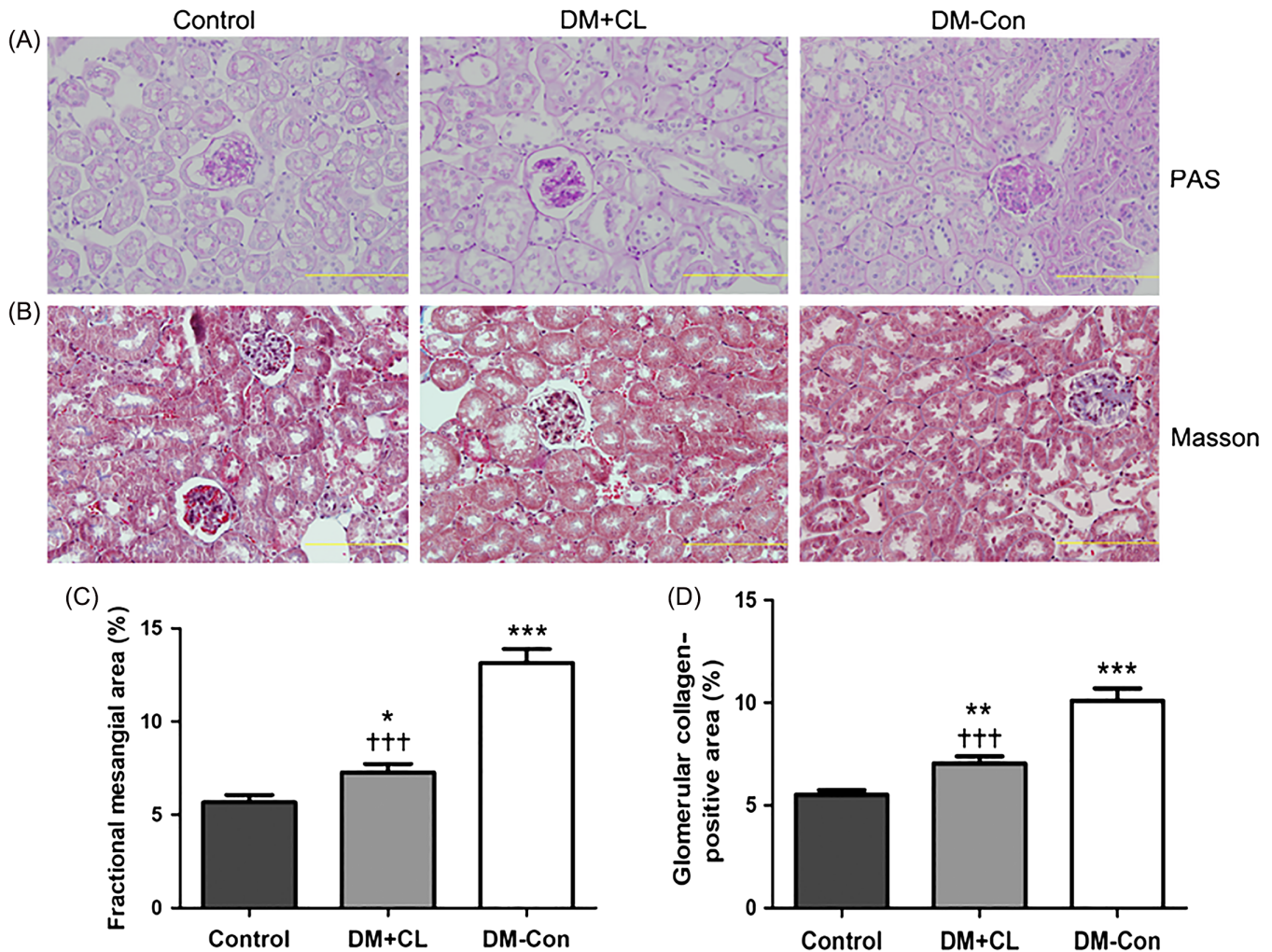


FIGURE 6 Legend on next column.



**FIGURE 7** Renal histological changes in non-diabetic (Control), streptozotocin-induced diabetic (DM-Con), and CL316,243-treated diabetic (DM + CL) mice. A,B, Representative images of periodic acid-Schiff (PAS) and Masson's trichrome (Masson) staining of renal sections from Control, DM-Con, and DM + CL mice. Bars, 10  $\mu$ m. C, Mesangial expansion and D, collagen accumulation in PAS- and Masson-stained slices, respectively, as quantified using Image-Pro Plus 6.0 software (Media Cybernetics, Silver Springs, MD). Data are the mean  $\pm$  SEM (n = 6 per group). \* $P$  < 0.05, \*\* $P$  < 0.01, \*\*\* $P$  < 0.001 compared with Control; ††† $P$  < 0.001 compared with the DM-Con group

This may be due to a variety of factors, including uncontrolled diabetic disorders, long-term HFD feeding, and drug-induced metabolic improvements and increased food intake. Conversely, Bartelt et al.<sup>22</sup> confirmed that activation of BAT could correct hyperlipidemia by modulating vascular lipoprotein homeostasis. In the present study, CL316,243-treated mice also exhibited changes in lipid profiles, including decreased serum TG and LDL-C concentrations.

In terms of DKD, we provide direct evidence that BAT activation significantly ameliorates albuminuria, renal fibrosis, and structural changes. In addition, CL316,243 treatment exhibited renal protective effects by improving in oxidative stress and inflammatory cytokines in the kidney. To further elucidate the potential mechanism independent of blood glucose control, we first detected the activity of interscapular BAT and epididymal adipose tissue. Numerous preclinical and clinical studies have reported that the role of BAT

**FIGURE 6** Fibrosis, inflammation, and oxidative stress-related molecules in the renal cortex of non-diabetic (Control), streptozotocin-induced diabetic (DM-Con), and CL316,243-treated diabetic (DM + CL) mice. A, Relative expression of the mRNA of renal fibrotic and inflammatory molecules. *Tgf- $\beta$ 1*, transforming growth factor- $\beta$ 1; *Col1*, collagen 1; *Fn*, fibronectin; *Tnf $\alpha$* , tumor necrosis factor- $\alpha$ ; *IL-1 $\beta$* , interleukin-1 $\beta$ . B, Representative western blot showing Fn, Col1, Tgf- $\beta$ 1, Tnf- $\alpha$ , NADPH oxidase 1 (Nox1), NAD(P)H dehydrogenase 1 (Nqo1), superoxide dismutase 1 (Sod1), and  $\beta$ -actin. C-I, Densitometric analysis of western blotting results. Data are the mean  $\pm$  SEM (n = 6 per group). \* $P$  < 0.05, \*\* $P$  < 0.01, \*\*\* $P$  < 0.001 compared with Control; † $P$  < 0.05, †† $P$  < 0.01 compared with the DM-Con group. <sup>a</sup> $P$  = 0.089 compared with the DM-Con group

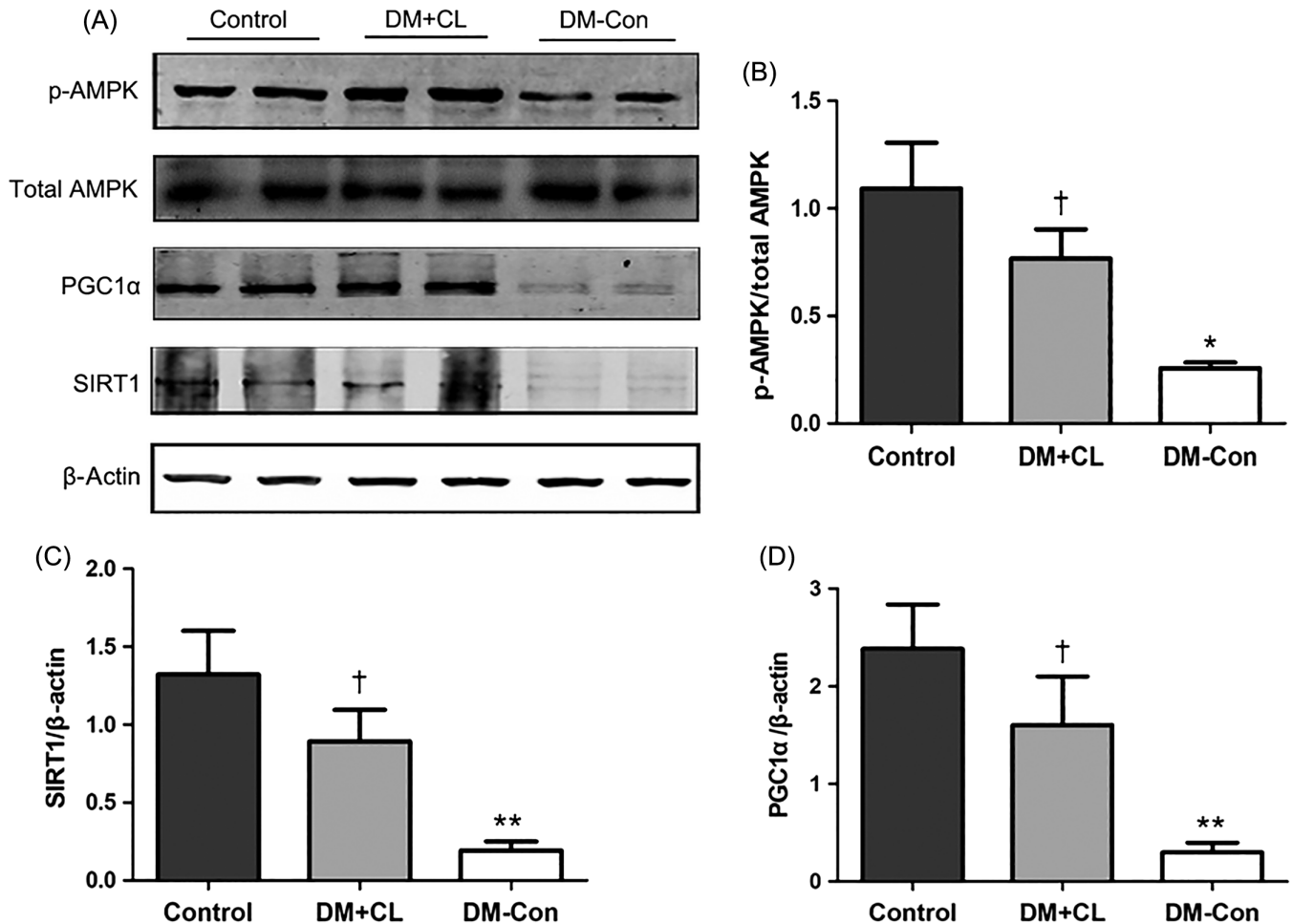


**FIGURE 8** Phosphorylated (p-) AMP-activated protein kinase (AMPK) (Thr<sup>172</sup>), total AMPK, sirtuin 1 (Sirt1) and peroxisome proliferator-activated receptor- $\gamma$  coactivator-1 $\alpha$  (Pgc1 $\alpha$ ) levels in the renal cortex of non-diabetic (Control), streptozotocin-induced diabetic (DM-Con), and CL316,243-treated diabetic (DM + CL) mice. A, Representative western blots for p-AMPK (Thr<sup>172</sup>), total AMPK, Sirt1, Pgc1 $\alpha$ , and  $\beta$ -actin in renal cortical tissues. B-D, Densitometric analysis of western blotting results. Data are the mean  $\pm$  SEM (n = 6 per group). \* $P$  < 0.05, \*\* $P$  < 0.01 compared with Control;  $\dagger P$  < 0.05 compared with DM-Con

gradually deteriorates in the development of obesity and diabetes.<sup>23,24</sup> In accordance with these data, we found that the expression of BAT-specific and fatty acid metabolism-related genes was downregulated in diabetic mice and restored by CL316,243 treatment. Next, we investigated whether these beneficial effects were mediated by BAT-secreted adipokines. Increasing evidence suggests that adiponectin reduces microalbuminuria and exerts renoprotective effects in diabetic animals.<sup>25</sup> The mechanism appears to be related to AMPK activation and an angiotensin-antagonistic effect.<sup>26,27</sup> In addition, low adiponectin levels in T2D patients are predictive of progression of DKD.<sup>28</sup> These findings are in agreement with the changes we observed in serum adiponectin concentrations observed in the present study. The potential mechanism may include the secretion of beneficial adipokines by refreshed BAT that then act on the kidney. Hondares et al.<sup>13</sup> recently reported that BAT could synthesize and secrete

Fgf21 after thermogenic activation. Elevated serum Fgf21 concentrations may be a useful indicator of kidney disease progression.<sup>29</sup> In the present study, we also observed a marked increase in serum Fgf21 concentrations in diabetic mice, suggesting that our diabetic model is an FGF21-resistant state. However, there was no change in serum FGF21 concentrations after BAT activation. To further explore how Fgf21 could act in the kidney, we tested Fgf21-related components, such as  $\beta$ -klotho and Fgfr1c. Interestingly, Fgf21-related components in the kidneys were markedly reduced following activation of BAT, suggesting that BAT activation enhances the sensitivity to Fgf21.

In eukaryotes, AMPK is a crucial kinase that primarily regulates energy metabolic homeostasis.<sup>30</sup> Both adiponectin and Fgf21 can activate the AMPK signaling pathway.<sup>26,31</sup> In the present study, we demonstrated that CL316,243 treatment activated the AMPK/Sirt1/Pgc1 $\alpha$  axis in the diabetic kidney. Accumulating data indicates that

activation of the AMPK/Sirt1/Pgc1 $\alpha$  pathway prevents inflammation and oxidative stress by inhibiting the nuclear factor- $\kappa$ B pathway and promoting fatty-acid  $\beta$ -oxidation, as well as the expression of antioxidants.<sup>32-34</sup> In addition, AMPK acts as an antifibrotic by reducing Nox4/Tgf- $\beta$ 1 signaling.<sup>35</sup> These possible mechanisms finally result in anti-oxidative stress, anti-inflammatory, and antifibrotic effects in the diabetic kidney following CL316,243 treatment.

Recently, BAT was reported to regulate hepatic metabolism by secreting miRNAs.<sup>4</sup> Coincidentally, miRNAs also play vital roles in the development of DKD.<sup>36</sup> The miRNAs may be another key medium between BAT and kidney. In the present study, BAT activation significantly upregulated some serum miRNAs and downregulated the renal expression of their related target genes, which are involved in the pathogenesis of DKD. In the present study we only focused on the mediums between BAT and the kidney, and we will explore the mechanisms by which these mediums act on the kidneys in the near future.

In summary, BAT activation has beneficial renal effects in diabetic mice by improving metabolic and activating renal AMPK/Sirt1/Pgc1 $\alpha$  signaling pathways. This may be mediated by effects of circulating BAT-derived adipokines and miRNAs on the kidney.

## ACKNOWLEDGEMENTS

We thank Min Yue at Laboratory Animal Center, Southern Medical University, Guangzhou, Guangdong, China for technical support.

## Disclosure

None declared.

## ORCID

Mei-Ping Guan  <https://orcid.org/0000-0002-9709-9320>

## REFERENCES

- Zoungas S, de Galan BE, Ninomiya T, et al. Combined effects of routine blood pressure lowering and intensive glucose control on macrovascular and microvascular outcomes in patients with type 2 diabetes: new results from the ADVANCE trial. *Diabetes Care*. 2009;32:2068-2074.
- Murea M, Freedman BI, Parks JS, Antinozzi PA, Elbein SC, Ma L. Lipotoxicity in diabetic nephropathy: the potential role of fatty acid oxidation. *Clin J Am Soc Nephrol*. 2010;5:2373-2379.
- Camara NO, Iseki K, Kramer H, et al. Kidney disease and obesity: epidemiology, mechanisms and treatment. *Nat Rev Nephrol*. 2017; 13:181-190.
- Thomou T, Mori MA, Dreyfuss JM, et al. Adipose-derived circulating miRNAs regulate gene expression in other tissues. *Nature*. 2017;542:450-455.
- Zhong X, Chung AC, Chen HY, et al. miR-21 is a key therapeutic target for renal injury in a mouse model of type 2 diabetes. *Diabetologia*. 2013;56:663-674.
- Walden TB, Hansen IR, Timmons JA, et al. Recruited vs. nonrecruited molecular signatures of brown, "brite," and white adipose tissues. *Am J Physiol Endocrinol Metab*. 2012;302: E19-E31.
- Ghorbani M, Claus TH, Himms-Hagen J. Hypertrophy of brown adipocytes in brown and white adipose tissues and reversal of diet-induced obesity in rats treated with a beta3-adrenoceptor agonist. *Biochem Pharmacol*. 1997;54:121-131.
- Wu C, Cheng W, Sun Y, et al. Activating brown adipose tissue for weight loss and lowering of blood glucose levels: a microPET study using obese and diabetic model mice. *PLoS One*. 2014;9: e113742.
- Cypess AM, Lehman S, Williams G, et al. Identification and importance of brown adipose tissue in adult humans. *N Engl J Med*. 2009;360:1509-1517.
- Cypess AM, Weiner LS, Roberts-Toler C, et al. Activation of human brown adipose tissue by a beta3-adrenergic receptor agonist. *Cell Metab*. 2015;21:33-38.
- Cypess AM, Haft CR, Laughlin MR, Hu HH. Brown fat in humans: consensus points and experimental guidelines. *Cell Metab*. 2014;20:408-415.
- Villarroya J, Cereijo R, Villarroya F. An endocrine role for brown adipose tissue? *Am J Physiol Endocrinol Metab*. 2013;305:E567-E572.
- Hondares E, Iglesias R, Giralt A, et al. Thermogenic activation induces FGF21 expression and release in brown adipose tissue. *J Biol Chem*. 2011;286:12 983-12 990.
- Kim HW, Lee JE, Cha JJ, et al. Fibroblast growth factor 21 improves insulin resistance and ameliorates renal injury in *db/db* mice. *Endocrinology*. 2013;154:3366-3376.
- Sakai T, Kusakabe T, Ebihara K, et al. Leptin restores the insulinotropic effect of exenatide in a mouse model of type 2 diabetes with increased adiposity induced by streptozotocin and high-fat diet. *Am J Physiol Endocrinol Metab*. 2014;307:E712-E719.
- Zheng Z, Guan M, Jia Y, et al. The coordinated roles of miR-26a and miR-30c in regulating TGFbeta1-induced epithelial-to-mesenchymal transition in diabetic nephropathy. *Sci Rep*. 2016;6: 37492.
- Xu P, Guan MP, Bi JG, Wang D, Zheng ZJ, Xue YM. High glucose down-regulates microRNA-181a-5p to increase pro-fibrotic gene expression by targeting early growth response factor 1 in HK-2 cells. *Cell Signal*. 2017;31:96-104.
- Sun X, Zhao S, Li H, et al. MicroRNA-30b suppresses epithelial-mesenchymal transition and metastasis of hepatoma cells. *J Cell Physiol*. 2017;232:625-634.
- Sun M, Hong S, Li W, et al. MiR-99a regulates ROS-mediated invasion and migration of lung adenocarcinoma cells by targeting NOX4. *Oncol Rep*. 2016;35:2755-2766.
- Guan M, Li W, Xu L, et al. Metformin improves epithelial-to-mesenchymal transition induced by TGF-beta1 in renal tubular epithelial NRK-52E cells via inhibiting Egr-1. *J Diabetes Res*. 2018;2018:1031367.

21. Wang D, Guan MP, Zheng ZJ, et al. Transcription factor Egr1 is involved in high glucose-induced proliferation and fibrosis in rat glomerular mesangial cells. *Cell Physiol Biochem*. 2015;36:2093-2107.
22. Bartelt A, Bruns OT, Reimer R, et al. Brown adipose tissue activity controls triglyceride clearance. *Nat Med*. 2011;17:200-205.
23. Seydoux J, Chinnet A, Schneider-Picard G, et al. Brown adipose tissue metabolism in streptozotocin-diabetic rats. *Endocrinology*. 1983;113:604-610.
24. van Marken LW, Vanhommerig JW, Smulders NM, et al. Cold-activated brown adipose tissue in healthy men. *N Engl J Med*. 2009;360:1500-1508.
25. Huang X, Su YX, Deng HC, Zhang MX, Long J, Peng ZG. Suppression of mesangial cell proliferation and extracellular matrix production in streptozotocin-induced diabetic mice by adiponectin in vitro and in vivo. *Horm Metab Res*. 2014;46:736-743.
26. Cammisotto PG, Bendayan M. Adiponectin stimulates phosphorylation of AMP-activated protein kinase alpha in renal glomeruli. *J Mol Histol*. 2008;39:579-584.
27. Guo X, Zhou G, Guo M, et al. Adiponectin retards the progression of diabetic nephropathy in *db/db* mice by counteracting angiotensin II. *Physiol Rep*. 2014;2:e230.
28. Kacso IM, Bondor CI, Kacso G. Plasma adiponectin is related to the progression of kidney disease in type 2 diabetes patients. *Scand J Clin Lab Invest*. 2012;72:333-339.
29. Lee CH, Hui EY, Woo YC, et al. Circulating fibroblast growth factor 21 levels predict progressive kidney disease in subjects with type 2 diabetes and normoalbuminuria. *J Clin Endocrinol Metab*. 2015;100:1368-1375.
30. Hardie DG. AMP-activated/SNF1 protein kinases: conserved guardians of cellular energy. *Nat Rev Mol Cell Biol*. 2007;8:774-785.
31. Chau MD, Gao J, Yang Q, et al. Fibroblast growth factor 21 regulates energy metabolism by activating the AMPK-SIRT1-PGC-1alpha pathway. *Proc Natl Acad Sci U S A*. 2010;107:12 553-12 558.
32. Xue B, Yang Z, Wang X, Shi H. Omega-3 polyunsaturated fatty acids antagonize macrophage inflammation via activation of AMPK/SIRT1 pathway. *PLoS One*. 2012;7:e45990.
33. Salminen A, Hyttinen JM, Kaarniranta K. AMP-activated protein kinase inhibits NF-kappaB signaling and inflammation: impact on healthspan and lifespan. *J Mol Med (Berl)*. 2011;89: 667-676.
34. Kim MY, Lim JH, Youn HH, et al. Resveratrol prevents renal lipotoxicity and inhibits mesangial cell glucotoxicity in a manner dependent on the AMPK-SIRT1-PGC1 $\alpha$  axis in *db/db* mice. *Diabetologia*. 2013;56:204-217.
35. Papadimitriou A, Peixoto EB, Silva KC, et al. Increase in AMPK brought about by cocoa is renoprotective in experimental diabetes mellitus by reducing NOX4/TGFBeta-1 signaling. *J Nutr Biochem*. 2014;25:773-784.
36. Bushati N, Cohen SM. microRNA functions. *Annu Rev Cell Dev Biol*. 2007;23:175-205.

**How to cite this article:** Cai Y-Y, Zhang H-B, Fan C-X, et al. Renoprotective effects of brown adipose tissue activation in diabetic mice. *Journal of Diabetes*. 2019;11:958–970. <https://doi.org/10.1111/1753-0407.12938>